

# Nanoscale Synergetic Effects on Ag–TiO<sub>2</sub> Hybrid Substrate for Photoinduced Enhanced Raman Spectroscopy (PIERS) with Ultra-Sensitivity and Reusability

Josiah Shondo, Salih Veziroglu, Tim Tjardts, Tamim Bin Sarwar, Yogendra Kumar Mishra, Franz Faupel,\* and Oral Cenk Aktas\*

Here, a 4N-in-1 hybrid substrate concept (nanocolumnar structures, nano-crack network, nanoscale mixed oxide phases, and nanometallic structures) for ultra-sensitive and reliable photo-induced-enhanced Raman spectroscopy (PIERS), is proposed. The use of the 4N-in-1 hybrid substrate leads to an ≈50-fold enhancement over the normal surface-enhanced Raman spectroscopy, which is recorded as the highest PIERS enhancement to date. In addition to an improved Raman signal, the 4N-in-1 hybrid substrate provides a high detection sensitivity which may be attributed to the activation possibility at extremely low UV irradiation dosage and prolonged relaxation time (long measurement time). Moreover, the 4N-in-1 hybrid substrate exhibits a superior photocatalytic degradation performance of analytes, allowing its reuse at least 18 times without any loss of PIERS activity. The use of the 4N-in-1 concept can be adapted to biomedicine, forensic, and security fields easily.

and biomolecules,<sup>[1]</sup> monitoring the environmental pollution and toxicity,<sup>[2]</sup> identification of narcotics and explosives, and detection of chemical and biological hazards within the forensic context<sup>[3,4]</sup> due to its ease of use and integration, chemical-specific detection capability, nondestructiveness, and label-free mode of operation.<sup>[5]</sup> In comparison to ordinary Raman spectroscopy, SERS provides a superior Raman intensity with an enhancement factor (EF) of several orders of magnitude, thanks to both the electromagnetic mechanism (EM) and chemical mechanism (CM) involved at the substrate surface.<sup>[6]</sup> EM arises basically from the localized surface plasmon resonance (LSPR) and CM results from the

chemical interactions (charge transfer and charge resonance) between the analyte molecules and the substrate surface.<sup>[7]</sup> EM is accepted as the primary SERS mechanism by providing an EF of 10<sup>7</sup>–10<sup>12</sup> through plasmonic metallic nanostructures, while CM leads to an EF of 10–10<sup>3</sup> and it acts as the secondary mechanism for SERS.<sup>[8,9]</sup>

The substrate plays the most critical role in the performance of SERS-based analytic techniques. The shape, orientation, and interspacing of plasmonic nanostructures on the SERS substrate greatly affect the SERS intensity and sensitivity since all these play a role on the interaction of light with the surface.<sup>[10,11]</sup> It has been shown that periodic metallic nanostructures provide more reproducible, uniform, and high-density hotspots on the substrate surface.<sup>[12]</sup> Although various advanced bottom-up and top-down fabrication methods and material combinations (1D, 2D, and 3D nanomaterials) have been demonstrated to prepare SERS active substrates, it is still challenging to achieve substrates with uniformly distributed hotspots and to maintain their stability against the analytes, solvents, and aging by the time.<sup>[13,14]</sup> In addition, time-consuming fabrication methods as well as single use nature of SERS substrates cause a high operational cost.

Apart from intense research going on the development of SERS substrates with high EFs and low-cost fabrication methods to produce such substrates, Parkin et al. reported totally a different approach which yields a significant enhancement of the Raman signal of analyte molecules on a metal–semiconductor hybrid substrate through preirradiating it by ultraviolet (UV) light (which is termed as photo-induced enhanced Raman

## 1. Introduction


Surface-enhanced Raman spectroscopy (SERS) has become a widely used analytical technique for the detection of biocides

J. Shondo, S. Veziroglu, T. Tjardts, T. B. Sarwar, F. Faupel, O. C. Aktas  
Chair for Multicomponent Materials  
Institute of Materials Science  
Faculty of Engineering  
Kiel University  
Kaiserstr. 2 24143, Kiel, Germany  
E-mail: ff@tf.uni-kiel.de; oca@tf.uni-kiel.de

S. Veziroglu, F. Faupel  
Kiel Nano, Surface and Interface Science KiNSIS  
Kiel University  
Christian Albrechts-Platz 4 24118, Kiel, Germany

Y. K. Mishra  
Mads Clausen Institute  
NanoSYD  
University of Southern Denmark  
Alsion 2, Sønderborg 6400, Denmark

O. C. Aktas  
Additive Manufacturing Excellence Centre – URTEMM  
Kahramankazan, Ankara 06980, Turkey

 The ORCID identification number(s) for the author(s) of this article can be found under <https://doi.org/10.1002/sml.202203861>.

© 2022 The Authors. Small published by Wiley-VCH GmbH. This is an open access article under the terms of the Creative Commons Attribution-NonCommercial-NoDerivs License, which permits use and distribution in any medium, provided the original work is properly cited, the use is non-commercial and no modifications or adaptations are made.

DOI: 10.1002/sml.202203861

spectroscopy—PIERS).<sup>[15]</sup> Basically, the preirradiation with UV light generates oxygen vacancies ( $V_O$ ) (through catalytic reactions with adsorbed  $O_2$  and  $H_2O$ ), and the  $V_O$  density increases with the irradiation time.<sup>[15–17]</sup> Various studies showed that the metal–oxide semiconductor interface can locate and stabilize  $V_O$ . Basically,  $V_O$  leads to the enhancement of the Raman signal through facilitating the charge transfer between the photo-irradiated oxide semiconductor film (decorated with metallic nanostructures) and analyte molecules via metallic nanostructures deposited on the surface (a semiconductor composed of  $V_O$  exhibits a valence state below the conduction band and this facilitates the charge transfer from  $V_O$  to the metallic nanostructures and then to the analyte molecule).<sup>[16]</sup> Li et al. showed that on a Ag– $TiO_2$  hybrid surface photogenerated electrons in  $TiO_2$  and the hot electrons injected (LSPR) from Ag nanostructures simultaneously promote the photocatalytic reactions and charge transfer to analyte molecules.<sup>[18]</sup> Therefore in metal–semiconductor hybrid substrates, the increase in the electron density (photogenerated) as well as the plasmonic nature of metallic nanostructures (LSPR) enhance the Raman scattering of analyte molecules.<sup>[19]</sup>

Following the pioneering work of Parkin's research group, various substrates including sole semiconductors and their combination with metallic nanostructures, have been studied to reveal their applicability as PIERS substrates.<sup>[15]</sup> The ultrafast recombination time ranging from picoseconds to microseconds hinders the use of semiconductors solely as PIERS substrate.<sup>[17]</sup> Semiconductors and even insulators decorated with metallic nanostructures have been shown as alternative PIERS substrates, but a large bandgap limits the PIERS performance since incident photon energy becomes insufficient to create adequate amount of oxygen vacancies.<sup>[20]</sup>

Combining metallic nanostructures with semiconductors such as  $TiO_2$  and ZnO, has been shown to trigger the formation of  $V_O$  with high density and stability.<sup>[12,21]</sup> Irradiation wavelength and duration also play an important role in the  $V_O$  formation.<sup>[22]</sup> The energy of the incident photons must be at least equal or even larger than the bandgap energy of the semiconductor substrate to induce  $V_O$  formation.  $V_O$  act as additional valence states below the conduction band edge of the semiconductor, and this facilitates the charge migration from the semiconductor to the metallic nanostructures.<sup>[23]</sup> Here,  $V_O$  is proportional to the irradiation time and the intensity, but very high irradiation dosages (irradiation intensity and/or time) can lead to vacancy healing and photo-induced bleaching of the analyte molecule, which decrease overall Raman detection performance.<sup>[24]</sup>

The performance of PIERS substrate also depends on the relaxation time; the intensity of the Raman signals decays gradually to the original level after the removal of light irradiation due to the recombination of electrons and holes.<sup>[17]</sup> Obviously, a longer relaxation time allows for efficient collection of Raman signals and reproducible measurements. Parkin et al. achieved an EF of 34.79 after exposing  $TiO_2$  surface decorated with Au nanostructures to UV light for extremely a long time interval (exceeding 240 min).<sup>[15]</sup> Zhang et al. reached EF of 27.8 by pre-irradiating Ag– $TiO_2$  surface with a mercury lamp operating at extremely high power (300 W) for 1–3 h.<sup>[25]</sup> In both cases, high EF was achieved by applying an extremely high irradiation

dosage, but this increases the risk of photo-induced (UV driven photochemical reactions) and/or photocatalytic (catalytic reactions induced by photogenerated electrons) bleaching of analytes.<sup>[26]</sup> On the other hand, if the photocatalytic bleaching of analyte molecules can be controlled, this may allow the reusability of PIERS substrates. But for such an approach, the metal–semiconductor hybrid substrate should be highly photocatalytically active to facilitate the generation of oxygen vacancies at extremely low UV irradiation dosage (otherwise, the use of high intensity irradiation will be needed, which is detrimental for organic analytes). Additionally, at such a low irradiation dosage, the relaxation time should still be long enough to conduct multiple measurements. Such a PIERS substrate can be simply cleaned up by increasing the UV irradiation slightly. For reusability of the PIERS substrate, one should also ensure the stability in terms of PIERS signal (position, intensity, and sensitivity) after several measurement cycles (analyte loading, measurement, and cleaning) and ideally, stability should be proven by employing different types of analytes for consecutive cycles.<sup>[27]</sup>

In the current study, we report on a significant enhancement of PIERS signal for Ag– $TiO_2$  hybrid substrate at extremely low UV irradiation dosage (with an irradiation intensity of  $4.5 \text{ mW cm}^{-2}$  and irradiation period of 8 min). We term this novel hybrid substrate, which leads to the enhancement of PIERS signal by a factor of around 50, as “4N-in-1 PIERS substrate.” In addition to the long relaxation time exceeding 240 min, the 4N-in-1 PIERS substrate exhibited an excellent reusability without any loss of PIERS activity after 18 cycles.

## 2. Results and Discussion

### 2.1. 4N-in-1 Hybrid Substrate and Characterization

Here 4N refers to i) nanocolumnar structures, ii) nanocrack network, iii) nanoscale mixed oxide phases, and iv) nanometallic structures (as depicted schematically in **Figure 1a**. Reactive sputtering and subsequently conducted heat treatment (heating and air quenching) led to the formation of columnar nanostructures and dense network of nanocracks, respectively. A critical temperature has been revealed to maximize the crack generation and promote the coexistence of rutile and anatase phases (which foster charge transfer and migration due to slight differences in their band gaps.<sup>[28]</sup> High photocatalytic nature of mentioned  $TiO_2$  film allows the controlled deposition of metallic Ag nanostructures under low-intensity UV irradiation, which prevents any agglomeration and excessive growth.

The 4N-in-1 hybrid substrate was prepared by a two-step process. First,  $TiO_2$  thin film with a thickness of 500 nm (composed of columnar nanostructures and nanocrack networks as shown in Figures 1b and 1c (Figure S1, Supporting Information), respectively) was prepared by reactive DC magnetron sputtering under relatively high oxygen partial pressure as reported earlier.<sup>[29,30]</sup> As we showed previously, subsequent heat treatment just after the sputtering led to the formation of networks of dense nanocracks and mixed rutile and anatase phases (Figure 1d and Figure S2, Supporting Information). We have shown that our sputter deposited  $TiO_2$  layer outperforms

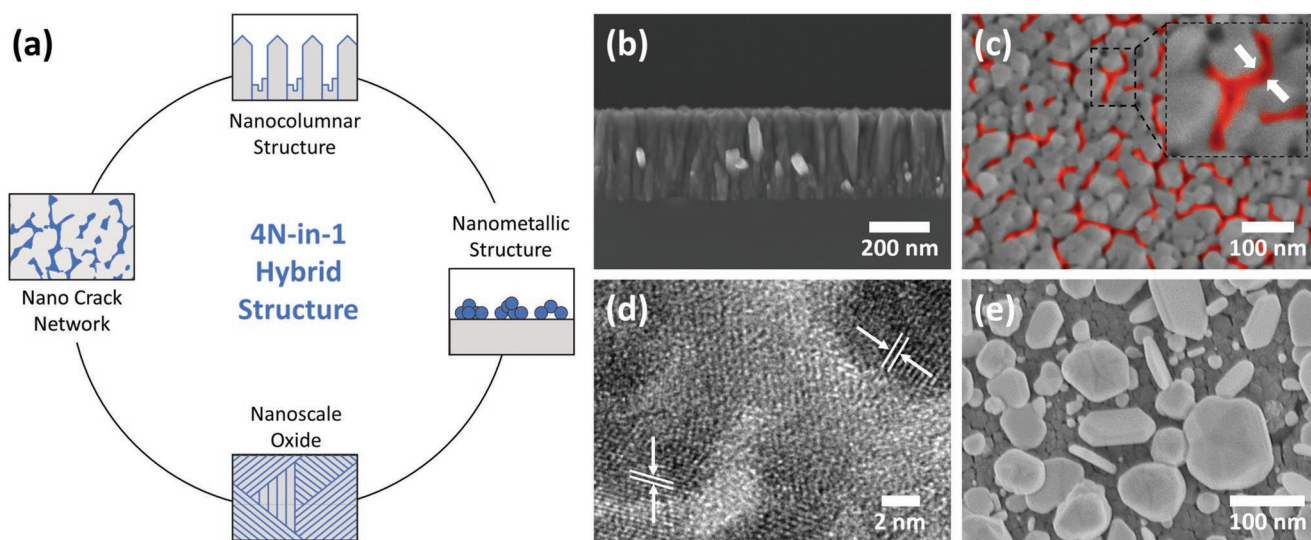


**Figure 1.** a) Schematic depicting 4N-in-1 PIERS substrate concept, b) cross-sectional SEM image of  $\text{TiO}_2$  nanocolumnar structures, c) SEM image of nanocracks networks on  $\text{TiO}_2$  thin film; (arrows indicate a crack size of 30–35 nm), d) HR-TEM images of mixed  $\text{TiO}_2$  phases (Anatase + Rutile phases are revealed by corresponding lattice spacings), and e) SEM images of  $\text{TiO}_2$  thin film decorated with Ag nanostructures (corresponding surface coverage is  $\approx 44.9\%$ ) via photocatalytic deposition.

well-known P25  $\text{TiO}_2$  nanoparticles, which are highly crystalline and have a high surface area of  $35\text{--}65\text{ m}^2\text{ g}^{-1}$  (as accepted as the golden standard to evaluate the photocatalytic activity of materials), by a factor of 29.5%.<sup>[29]</sup> As a second step, Ag nanostructures were reduced (from an aqueous solution of  $\text{AgNO}_3$ ) preferentially on  $\text{TiO}_2$  thin film surface via the photocatalytic deposition process developed earlier.<sup>[31]</sup> Following the irradiation of  $\text{TiO}_2$  thin film surface with UV light operating at a wavelength of 365 nm and a power of  $4.5\text{ mW cm}^{-2}$  for 20 min, photogenerated electrons reduced  $\text{Ag}^+$  ions to stable  $\text{Ag}^0$  (metallic silver) on the  $\text{TiO}_2$  thin film surface. The prepared 4N-in-1 hybrid surface morphology is visualized by scanning electron microscopy (SEM) analysis as shown in Figure 1e. One can alter the surface coverage of Ag% on the  $\text{TiO}_2$  thin film surface simply by increasing the photocatalytic deposition time as shown in Figure S3, Supporting Information. The possibility of using low UV irradiation (thanks to the high photocatalytic activity of  $\text{TiO}_2$  thin film) seems to be effective in hindering the growth within the solution and uncontrolled agglomeration of Ag particles on  $\text{TiO}_2$  surface. We conducted X-ray photoelectron spectroscopy (XPS) to determine the surface chemistry of the prepared 4N-in-1 hybrid substrates with different Ag% surface coverage. For all samples, we observed that Ag 3d spectra consists of two peaks corresponding to Ag  $3d_{3/2}$  and Ag  $3d_{5/2}$  with a binding energy difference of  $\approx 6.0\text{ eV}$ , which clearly proves the formation of stable metallic Ag (Figure S4, Supporting Information).<sup>[32]</sup> In Figure S4, Supporting Information, one can see that Ti 2p spectra are composed of two prominent characteristic peaks known as Ti  $2p_{1/2}$  and Ti  $2p_{3/2}$ , respectively.<sup>[31]</sup> The distance between these two peaks is  $\approx 5.6\text{ eV}$  in case of bare  $\text{TiO}_2$ , which can be attributed to the  $\text{Ti}^{4+}$  state indicating the formation of stable  $\text{TiO}_2$ .<sup>[33,34]</sup> On the other hand, it can be clearly seen from high-resolution XPS spectra of Ti 2p (Figure S4, Supporting Information), that increasing Ag content on the surface causes a positive shift of the two-distinct Ti 2p peaks. Pei et al.

reported a positive shift in Ti 2p which may be attributed to defective  $\text{Ti}^{3+}$  structure.<sup>[35]</sup> In principle,  $\text{V}_\text{O}$  transfer their extra two electrons to the adjacent two  $\text{Ti}^{4+}$  atoms to form  $\text{Ti}^{3+}$ .<sup>[36,37]</sup> Here the increase in the amount of  $\text{V}_\text{O}$  with the increase in Ag% on the surface can be explained by the growth of Ag– $\text{TiO}_2$  interface.<sup>[38]</sup>

Furthermore, the O 1s spectrum originated from adsorbed oxygen, hydroxyl groups, and lattice oxygen are also shown in Figure S4, Supporting Information.<sup>[39]</sup> This clearly shows that increasing of Ag content on  $\text{TiO}_2$  surface promotes the adsorption of higher amounts of oxygen and hydroxyl groups which certainly also plays a role in the formation and stabilization of  $\text{V}_\text{O}$ .<sup>[40]</sup> On the other hand, we did not see any oxidation on Ag particles since satellite peaks at 366 eV (Figure S4, Supporting Information). This also explains that the increase in adsorbed oxygen amount (O 1s spectra) should be related to the change in the state of  $\text{Ti}^{4+}$  (increase in the amount of  $\text{V}_\text{O}$  and transformation of  $\text{Ti}^{4+}$  state to  $\text{Ti}^{3+}$ ).

## 2.2. PIERS Analysis and Mechanism

To demonstrate the PIERS performance of the 4N-in-1 hybrid substrate, we conducted two consecutive SERS measurements with and without applying a UV pre-irradiation step. For PIERS, we exposed the 4N-in-1 hybrid substrate to the UV-LED light source operating at a wavelength of 365 nm for 8 min. Afterward,  $10\text{ }\mu\text{L}$  of ethanolic solution of Rhodamine 6G analyte ( $\text{R6G} \approx 10^{-7}\text{ M}$ ) was drop-casted on 4N-in-1 hybrid substrate, and the sample was dried in the dark for 10 min. Similarly, we loaded the same analyte on another 4N-in-1 hybrid substrate and allowed it to dry in the dark for also 10 min. The intensity difference of PIERS and SERS spectra recorded at an integration time of 5 s (using a laser source operating at a wavelength of 532 nm and an intensity of  $15\text{ }\mu\text{W}$ ) is shown in Figure 2a;



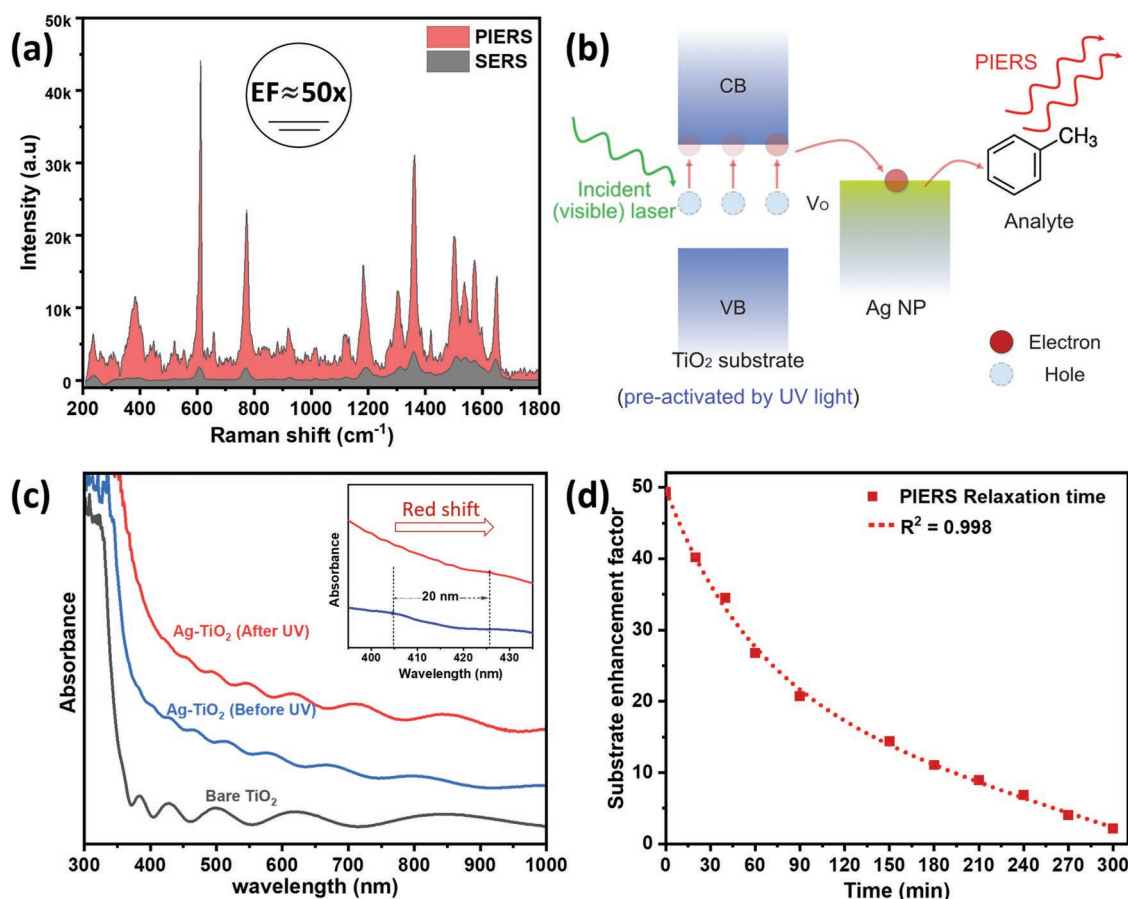


**Figure 2.** a) Comparison of PIERS and SERS performance of 4N-in-1 hybrid substrate for the detection of trace amount of RG6 analyte ( $\approx 10^{-7}$  molar), b) PIERS mechanism for 4N-in-1 hybrid substrate, c) comparison of UV-vis absorbance spectra of 4N-in-1 hybrid substrate before and after UV irradiation (inset shows the red-shift), and d) relaxation curve (decay of the PIERS signal) after removing UV irradiation.

there is a significant enhancement in terms of Raman signal intensity through UV irradiation. The Raman intensity of the peak located at 611 cm<sup>-1</sup> increases from 894 to 44 098 cps, which is around 50-fold (depending on the distribution density of Ag nanostructures, slight differences can be seen in enhancement in Raman signals recorded from different position on 4N-in-1 PIERS substrate as shown in Figure S5, Supporting Information). Our systematic study showed that EF is proportional to preirradiation time (Figure S6, Supporting Information) but we achieved the highest EF (which corresponds to the highest photoinduced charge generation) between 5 and 10 min. In general, the rate of a photocatalytic reaction is proportional to the irradiation flux (high irradiation flux generates high number of photo-induced electrical charges). On the other hand, above a certain value (estimated to be  $\approx 25$  mW cm<sup>-2</sup>) the reaction rate reaches a saturation;<sup>[41]</sup> similarly we observed that longer irradiation period (>10 min) does not lead to further enhancement in Raman signal (Figure S6, Supporting Information).

Similar like commercial SERS substrates, 4N-in-1 hybrid substrate also exhibits a significant enhancement in Raman signal without any preirradiation by UV (which can be referred as classical SERS enhancement). However, after UV preirradiation 4N-in-1 hybrid substrate (in PIERS mode) exhibits a superior detection capability (R6G prepared at  $\approx 10^{-7}$  M) in comparison

to commercial SERS substrates (Figure S7, Supporting Information). Detection limit of 4N-in-1 hybrid structure can be extended to very low concentrations around  $10^{-14}$  M as demonstrated at Figure S8, Supporting Information.

While in classical SERS, Raman signal enhancement is mainly determined by the LSPR of metallic nanostructures on the surface, in PIERS, an additional enhancement comes from the UV induced charge migration from the semiconductor substrate to the metallic nanostructures as schematically depicted in Figure 2b. Various studies showed that the metal-oxide interface can locate and stabilize V<sub>O</sub>.<sup>[16,42]</sup> Here, the production of V<sub>O</sub> permits enhancing the Raman signal of chemical molecules through charge transfer processes between the photo-irradiated TiO<sub>2</sub> film and analyte molecules via metallic Ag nanostructures.<sup>[16]</sup> High-resolution XPS spectra of Ti 2p (at Figure S4, Supporting Information) shows that increasing Ag content on the surface causes a positive shift of two-distinct Ti 2p peaks, which may indicate indirectly the presence of V<sub>O</sub>.<sup>[35]</sup> The increase in the amount of V<sub>O</sub> with the increase in Ag% on the surface can be explained by the growth of Ag-TiO<sub>2</sub> interface. Figure S9, Supporting Information, shows initial increasing of the surface coverage ( $\approx 6.3\%$ ) has significant effect on the PIERS enhancement which may be correlated with the formation and as well as the stabilization of V<sub>O</sub>. However,

further increase in Ag surface coverage (>44.9%) enhances the reflection therefore reduces the absorption of the light by  $\text{TiO}_2$ <sup>[26]</sup> and this seems to hinder further PIERS enhancement (Figure S9, Supporting Information).

To further reveal the mechanism of PIERS effects, we measured absorption spectra of 4N-in-1 hybrid substrate before and after the UV irradiation. We observed an apparent increase in the overall absorption and a clear red-shift of LSPR band from 405 to 425 nm after the UV irradiation (Figure 2c). Here red-shift in the 4N-in-1 hybrid substrate can be attributed to the increased electron density on Ag nanostructures covering  $\text{TiO}_2$ .<sup>[40]</sup> Therefore definitely hot electrons play also a major role for achieving high EFs in PIERS. We believe that there is a synergistic effect of the i) plasmonic nature of Ag nanostructures (hot electrons), ii) Schottky barrier at the Ag- $\text{TiO}_2$  interface, and iii)  $\text{V}_\text{O}$  stabilization at the Ag- $\text{TiO}_2$  interface.

Since PIERS leads to diverse EFs for different analytes and even for different Raman bands for the same analytes, one needs to take this into account to conduct reliable comparison between different measurements (Table S1, Supporting Information). For instance, while Parkin et al. showed an EF of 2.76 (PIERS to SERS signal ratio at a peak position of  $610\text{ cm}^{-1}$ ) for rhodamine 6G, we achieved an EF of 49.58 by using the same analyte prepared at identical molarity.<sup>[15]</sup> The decay of PIERS intensity to its original state lasted longer than 240 min, as shown in Figure 2d, which clearly indicates a very slow vacancy healing in air. Such a long relaxation time is ideal to get reproducible and highly sensitive measurements (4N-in-1 hybrid substrate exhibited around four to five times longer relaxation time in comparison to reported values to the date.<sup>[15,21,43]</sup> Here extremely high EF difference between ours and those reported so far can be attributed to high photocatalytic activity of 4N-in-1 hybrid substrate.

In addition to the PIERS effect, the proposed 4N-in-1 hybrid substrate can decompose organic molecules by applying UV-irradiation (either by using high intensity UV light or conducting a prolonged UV-irradiation time). 4N-in-1 hybrid substrate shows superior decomposition performance of analyte

compared to commercial SERS substrate due to its highly active photocatalytic nature (Figure S10, Supporting Information). Therefore, by simply exposing the analyte deposited 4N-in-1 hybrid substrate to UV light source (operating at 365 nm) just after collecting Raman spectra, we decomposed the analyte fully, and this allows the reuse of the 4N-in-1 hybrid substrate.

### 2.3. Reusability for PIERS Analysis

To demonstrate the reusability of the proposed hybrid substrate first, after the UV preirradiation we contaminated the surface by drop casting 10  $\mu\text{L}$  of dilute (molarity  $\approx 10^{-7}\text{ M}$ ) R6G solution. Then we collected the Raman signal from the surface, and finally, we exposed the substrate to a high intensity ( $10\text{ mW cm}^{-2}$ ) UV light to clean up the surface totally (clean-up time depends on the amount of the analyte adsorbed on the surface as shown in Figure S11, Supporting Information). The UV preirradiation can be termed as the activation step, and other consecutive steps such as loading of the analyte, collecting the Raman spectra and the photocatalytic decomposition of analyte (this can be given as a single cycle as shown schematically in Figure 3a). We showed the self-cleaning process by the UV irradiation and reversible Raman activity in Figure 3b. PIERS activity could be restored after the simple UV cleaning step, and the same substrate could be reused at least 18 times without any loss of PIERS activity, which clearly indicates an excellent reusability. Even after some cycles, we observed that the PIERS signal exceeded its original value, which can be easily explained by consecutively repeated UV irradiation (cumulative activation) for every cycle. When we compare the reusability of 4N-in-1 hybrid surface with those proposed by Parkin et al. and Zhang et al. (surfaces fail after five and 15 times use, respectively) it is clearly seen that our hybrid substrate exhibits extremely high stability after multiple measurements.<sup>[15,21]</sup> Therefore, our hybrid surface may act as reliable (see comparison Table S1, Supporting Information) PIERS platform for multiple detection.

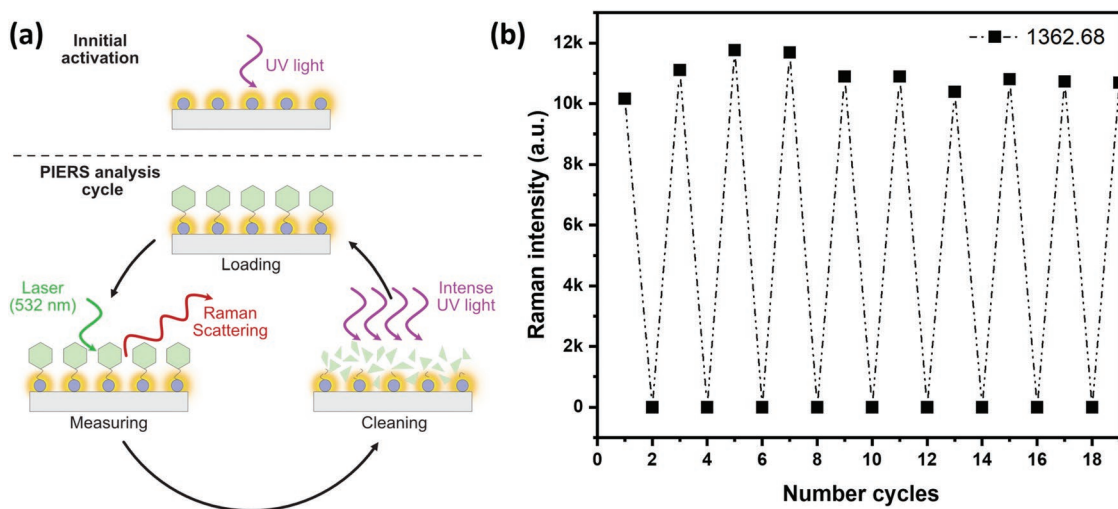


**Figure 3.** a) Schematic depiction of initial PIERS activation and PIERS analysis cycle, and b) reusability of 4N-in-1 hybrid substrate for multiple PIERS analysis.

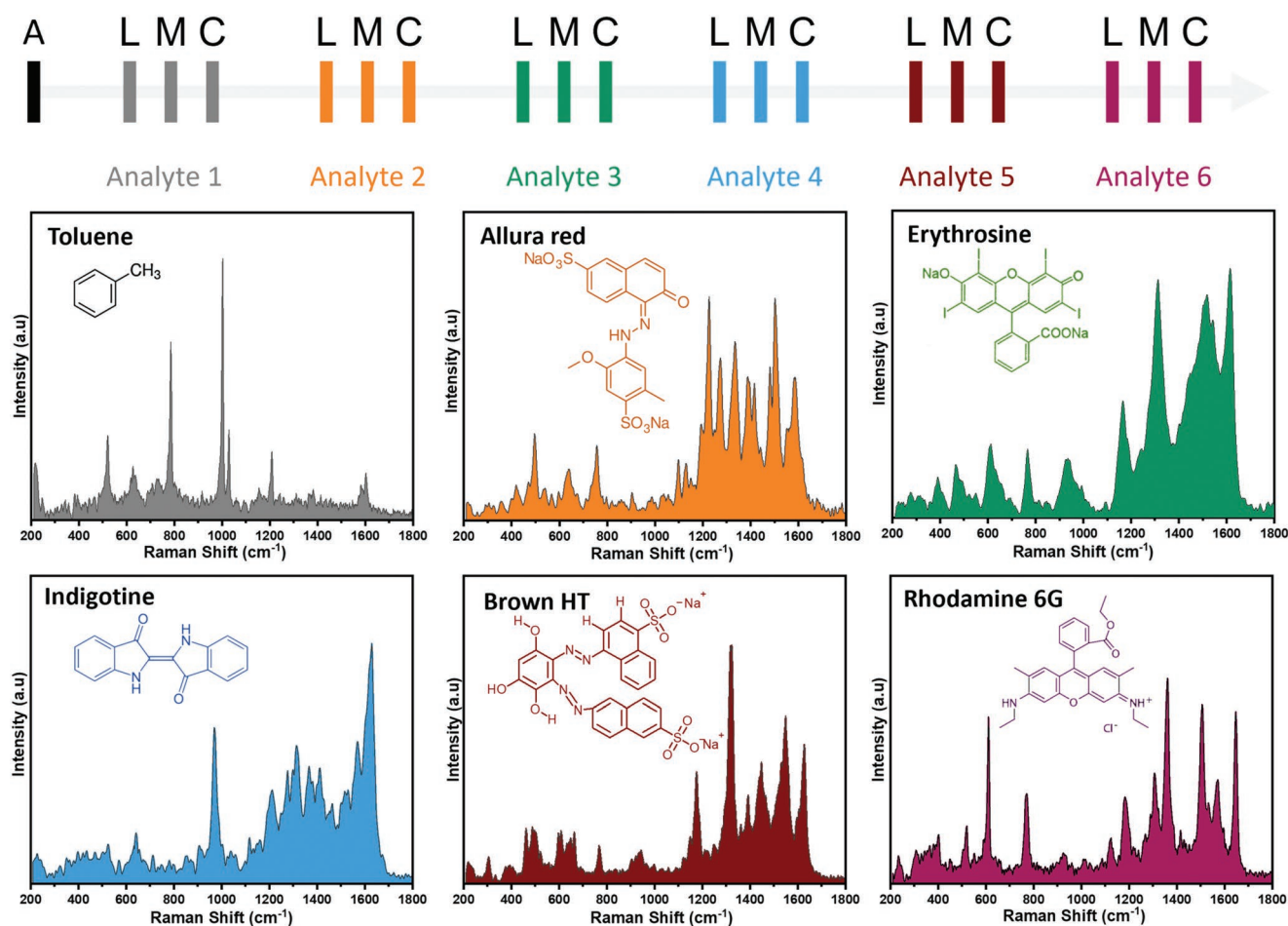


**Figure 4.** Illustration of PIERS initial activation and consecutive six PIERS analysis cycles for six different analytes with corresponding PIERS spectra (Toluene, Allura red, Erythrosine, Indigo tine, Brown HT, and Rhodamine 6G). (A: PIERS Activation, L: PIERS Analyte Loading, M: PIERS Measurement, and C: PIERS Cleaning)

To further demonstrate the reusability of 4N-in-1 hybrid substrate for multiple PIERS analysis, the same substrate was subjected to six consecutive loading-measurement-clean up cycles (following initial activation step) and for every cycle, a new type of analyte (first cycle: Toluene, second cycle: Allura red, third cycle: Erythrosine, fourth cycle: Indigotine, fifth cycle: Brown HT, and sixth cycle: Rhodamine 6G) was loaded. As presented in **Figure 4**, we were able to detect all characteristics peaks for each analyte without loss of any analyte signal and position (as shown in detail in Table S2, Supporting Information). This proves that the 4N-in-1 hybrid substrate can preserve its specificity and reusability after the photocatalytic clean-up.

## 2.4. Vapor Phase PIERS Analysis

To reveal how the sensitivity was improved by our PIERS approach in comparison to normal SERS, we compared the detection capabilities of both methods to monitor the surface contamination induced also by a vapor phase analyte. In a typical experiment, 10  $\mu\text{L}$  of vinyl chloride ( $\approx 10 \text{ ng mL}^{-1}$ ) was diluted in a methanol solution. The UV preirradiated

substrate was held at 5 cm above the prepared solution, as schematically illustrated in **Figure 5a**. Afterward, the PIERS signal was acquired, and similarly, the SERS signal was recorded without the UV preirradiation step for comparison. As shown in **Figure 5b**, 4N-in-1 hybrid substrate exhibited a PIERS signal which is 20 times higher than that recorded by SERS (all characteristic peaks of vinyl chloride recorded by PIERS and SERS are given in Table S3, Supporting Information).

In conclusion, we proposed an ultrasensitive and reliable PIERS active substrate termed as “4N-in-1 PIERS substrate” based on Ag-TiO<sub>2</sub> hybrid structures. Upon UV irradiation, we achieved a PIERS enhancement up to 50 times in comparison to normal SERS intensity. In addition to improved Raman signal, 4N-in-1 hybrid substrate provided a high detection sensitivity which may be attributed to the activation possibility with an extremely low incident photon energy and prolonged relaxation time. Moreover, 4N-in-1 hybrid substrate showed a superior photocatalytic degradation performance of analytes, allowing its reuse at least for 18 cycles without any loss of PIERS activity. Our 4N-in-1 hybrid substrate concept can be combined with any type of Raman spectroscopy by simply integrating a UV light



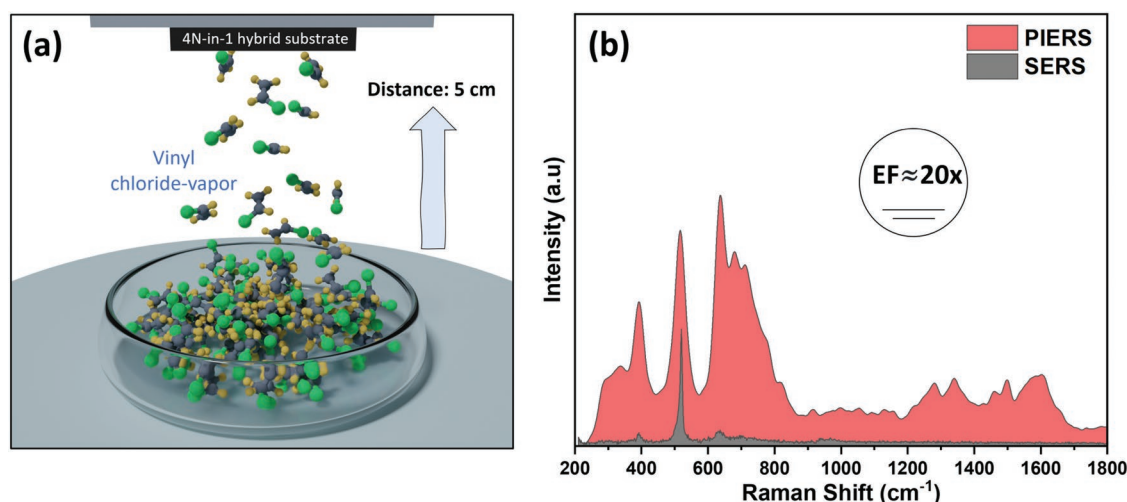


**Figure 5.** a) Schematic illustration of the detection of vapor phase analyte and b) a comparative analysis of vapor phase analyte by PIERS and SERS.

source, and this may trigger new applications for biomedicine, forensic, and security fields (a possible case is shown in Figure S12, Supporting Information)

### 3. Experimental Section

**Materials and Methods:** Silver nitrate (99.999%), rhodamine 6 g (99.8%), methyl alcohol (99.99%), ethyl alcohol (99.8%), 1-methyl-4-nitrobenzene (99%), vinyl chloride solution (2000  $\mu\text{g mL}^{-1}$  in methanol), and methylbenzene (anhydrous 99.8%), were obtained from Sigma-Aldrich, Germany. Allura red, Erythrosine, Brown HT, and Indigotin were obtained from FastColours LLP, UK.

**Preparation of TiO<sub>2</sub> Thin film:** The deposition of 500 nm thick TiO<sub>2</sub> thin film was carried out using direct current magnetron sputtering from a titanium (Ti) target in a custom-built vacuum deposition chamber as previously reported.<sup>[30,44,45]</sup> Silicon wafer pieces (10 mm × 10 mm) were used as substrate. Before the deposition of TiO<sub>2</sub> thin film, the chamber was conditioned to reach a base pressure of 10<sup>-5</sup> Pa using a rotary pump (Agilent Technologies, SH-110) in combination with a molecular turbopump (Pfeiffer Vacuum, HiPace 400). First, the Ti target (Goodfellow, 99.99% of 50 mm diameter) was cleaned in a pure Ar plasma for 10 min. Afterward, the deposition was carried out (for 65 min) under a gas mixture of Ar and O<sub>2</sub> (at a ratio of 250:5 maintained by using two separate mass flow controllers-MKS Multi-Gas-Controller 647C) and at a magnetron output power of 120 W. A homogeneous TiO<sub>2</sub> film was achieved by rotating an automated sample holder during the deposition. Afterward, the prepared thin films were annealed for an hour at 650 °C in an oven (Nabertherm, LE 4/11/R6) and subsequently air quenched to induce a nano-cracks network (leading to high surface area), as was reported previously.<sup>[29]</sup>

**Photocatalytic Deposition of Ag Nanostructures on TiO<sub>2</sub> Thin Film:** In a typical experiment, 6.5 mL of silver nitrate ( $\text{AgNO}_3 = 1 \times 10^{-3} \text{ M}$ ) was filled in methanol, a UV-transparent quartz cuvette as was described in detail previously.<sup>[45]</sup> Afterward, prepared TiO<sub>2</sub> thin film samples were dipped into the quartz cuvette and exposed to low-intensity (operating at a wavelength of 365 nm and a power of 4.5 mW cm<sup>-2</sup>) UV light (UV LED StellarNet EPP2000C-SR-50) for 20 min. Then, samples were rinsed with deionized water to remove excess solution and left to dry at room temperature.

**Scanning Electron Microscopy (SEM):** The surface morphology of prepared samples was analyzed with SEM (Supra55VP-Carl Zeiss) at an accelerating voltage of 3 kV (with 3 mm working distance).

**X-ray Photoelectron Spectroscopy (XPS):** XPS (using Omicron Nano-Technology GmbH, Al anode, 240 W) was employed to determine the chemical state on the surface. CasaXPS software (2.3.13PR1.0) was used for quantitative analysis and detailed peak investigation. All binding energies (BE) were referenced according to the C 1s line at 285 eV (originates from adventitious carbon on the sample surface).

**UV-Vis Measurement:** For UV-vis analysis, 500 nm thick TiO<sub>2</sub> film was deposited on quartz pieces (10 mm × 10 mm), and these samples were annealed at 650 °C for an hour. Then, prepared samples were fixed onto a custom-designed optical holder for UV-vis analysis. UV-vis spectra were collected within the 200–1000 nm wavelength range at a scanning rate of 2 nm s<sup>-1</sup> using a spectrophotometer (PerkinElmer LAMBDA-900, Made in Germany). The quartz glass spectrum was used for the baseline correction.

**Raman Measurement:** Raman Spectroscopy analysis was conducted using a commercially available confocal Raman microscope (WITec alpha300 RA, Ulm, Germany) equipped with an Nd: YAG 532 nm laser source. Intensity calibration was performed using a silicon wafer via the most significant silicon mode at 520 cm<sup>-1</sup>. All SERS and PIERS spectra were acquired using 1200 g mm<sup>-1</sup> BLZ 300NM grating at the excitation source power of 15  $\mu\text{W}$ .

To acquire the Raman signal of the individual analytes, a fixed volume of 10  $\mu\text{L}$  of analyte was drop-cast onto the Ag decorated TiO<sub>2</sub> and allowed to dry in air for 10 min. Typically, SERS spectra were acquired without UV preirradiation step. On the other hand, in PIERS data acquisition, 10  $\mu\text{L}$  of the analyte was deposited on the UV preirradiated samples and allowed to dry in air for 10 min and kept in the dark.

### Supporting Information

Supporting Information is available from the Wiley Online Library or from the author.

### Acknowledgements

J.S. and S.V. contributed equally to this work. J.S. thanks the Petroleum Technology Development Fund (PTDF) and the Deutscher Akademischer Austauschdienst (DAAD) for providing funding for his doctoral studies. This work is financially supported by the Deutsche Forschungsgemeinschaft (DFG, German Research Foundation)- project number 448935424 i.e., project FA234/35-1. The authors thank NanoBMT Co. Ltd. for preparing of some analytes.

Open Access funding enabled and organized by Projekt DEAL.

## Conflict of Interest

The authors declare no conflict of interest.

## Data Availability Statement

The data that support the findings of this study are available in the supplementary material of this article.

## Keywords

hybrid structures, photocatalysis, reusability, surface-enhanced Raman spectroscopy, ultra-sensitivity

Received: June 22, 2022

Revised: August 26, 2022

Published online: September 22, 2022

- [1] A. J. M. Fleischmann, P. J. Hendra Mcquillan, *Chem. Phys. Lett.* **1974**, 26, 163.
- [2] J. Langer, D. J. de Aberasturi, J. Aizpurua, R. A. Alvarez-Puebla, B. Augu  , J. J. Baumberg, G. C. Bazan, S. E. J. Bell, A. Boisen, A. G. Brolo, J. Choo, D. Cialla-May, V. Deckert, L. Fabris, K. Faulds, F. J. Garc  a de Abajo, R. Goodacre, D. Graham, A. J. Haes, C. L. Haynes, C. Huck, T. Itoh, M. K  ll, J. Kneipp, N. A. Kotov, H. Kuang, E. C. Le Ru, H. K. Lee, J. F. Li, X. Y. Ling, et al., *ACS Nano* **2020**, 14, 28.
- [3] C. Andreou, M. R. Hoonejani, M. R. Barmi, M. Moskovits, C. D. Meinhart, *ACS Nano* **2013**, 7, 7157.
- [4] H. Dies, J. Raveendran, C. Escobedo, A. Docoslis, *Sens. Actuators B Chem.* **2018**, 257, 382.
- [5] T. K. Naqvi, A. Bajpai, M. S. S. Bharati, M. M. Kulkarni, A. M. Siddiqui, V. R. Soma, P. K. Dwivedi, *J. Hazard. Mater.* **2021**, 407, 124353.
- [6] Y. S. Yamamoto, Y. Ozaki, T. Itoh, *J. Photochem. Photobiol. C* **2014**, 21, 81.
- [7] K. A. Willets, R. P. Van Duyne, *Annu. Rev. Phys. Chem.* **2007**, 58, 267.
- [8] L. Guerrini, D. Graham, *Chem. Soc. Rev.* **2012**, 41, 7085.
- [9] B. N. J. Persson, K. Zhao, Z. Zhang, *Phys. Rev. Lett.* **2006**, 96, 207401.
- [10] R. Pilot, R. Signorini, C. Durante, L. Orian, M. Bhamidipati, L. Fabris, *Biosensors* **2019**, 9, 57.
- [11] S. Gullace, V. Montes-Garc  a, V. Mart  n, D. Larios, V. Girelli Conso-laro, F. Obelleiro, G. Calogero, S. Casalini, P. Samor  , *Small* **2021**, 17, 2100755.
- [12] A. Fularz, S. Almohammed, J. H. Rice, *ACS Appl. Nano Mater.* **2020**, 3, 1666.
- [13] J. Chen, H. Su, X. You, J. Gao, W. M. Lau, D. Zhang, *Mater. Res. Bull.* **2014**, 49, 560.
- [14] S. Zhao, H. Wang, L. Niu, W. Xiong, Y. Chen, M. Zeng, S. Yuan, L. Fu, *Small* **2021**, 17, 2103442.
- [15] S. Ben-Jaber, W. J. Peveler, R. Quesada-Cabrera, E. Cort  s, C. Sotelo-Vazquez, N. Abdul-Karim, S. A. Maier, I. P. Parkin, *Nat. Commun.* **2016**, 7, 12189.
- [16] G. Barbillon, *Materials* **2021**, 14, 4423.
- [17] D. Glass, E. Cort  s, S. Ben-Jaber, T. Brick, W. J. Peveler, C. S. Blackman, C. R. Howle, R. Quesada-Cabrera, I. P. Parkin, S. A. Maier, *Adv. Sci.* **2019**, 6, 1901841.
- [18] L. Li, L. Song, L. Zhu, Z. Yan, X. Cao, *Catal. Sci. Technol.* **2018**, 8, 1277.
- [19] T. Bora, in *Noble and Precious Metals - Properties, Nanoscale Effects and Applications* (Eds: M. S. Seehra, A. D. Bristow), IntechOpen, London **2018**, pp. 118–129.
- [20] S. Cong, Y. Yuan, Z. Chen, J. Hou, M. Yang, Y. Su, Y. Zhang, L. Li, Q. Li, F. Geng, Z. Zhao, *Nat. Commun.* **2015**, 6, 7800.
- [21] M. Zhang, H. Sun, X. Chen, J. Yang, L. Shi, T. Chen, Z. Bao, J. Liu, Y. Wu, *ACS Sens.* **2019**, 4, 1670.
- [22] J. Zhao, Z. Wang, J. Lan, I. Khan, X. Ye, *Nanoscale* **2021**, 13, 8707.
- [23] R. Kavitha, S. G. Kumar, *Chem. Pap.* **2020**, 74, 717.
- [24] H. Yamashita, M. Harada, J. Misaka, M. Takeuchi, K. Ikeue, M. Anpo, *J. Photochem. Photobiol. A Chem.* **2002**, 148, 257.
- [25] M. Zhang, H. Sun, X. Chen, J. Yang, T. Chen, Z. Bao, J. Liu, Y. Wu, *ACS Sens.* **2019**, 4, 1670.
- [26] S. Veziroglu, A.-L. Obermann, M. Ullrich, M. Hussain, M. Kamp, L. Kienle, T. Le  sner, H.-G. Rubahn, O. Polonskyi, T. Strunskus, J. Fiutowski, M. Es-Souni, J. Adam, F. Faupel, O. C. Aktas, *ACS Appl. Mater. Interfaces* **2020**, 12, 14983.
- [27] X. Jiang, X. Sun, D. Yin, X. Li, M. Yang, X. Han, L. Yang, B. Zhao, *Phys. Chem. Chem. Phys.* **2017**, 19, 11212.
- [28] B. Henkel, T. Neubert, S. Zabel, C. Lamprecht, C. Selhuber-Unkel, K. R  tzke, T. Strunskus, M. Verg  hl, F. Faupel, *Appl. Catal. B* **2016**, 180, 362.
- [29] M. Z. Ghorri, S. Veziroglu, B. Henkel, A. Vahl, O. Polonskyi, T. Strunskus, F. Faupel, O. C. Aktas, *Sol. Energy Mater. Sol. Cells* **2018**, 178, 170.
- [30] A. Vahl, S. Veziroglu, B. Henkel, T. Strunskus, O. Polonskyi, O. C. Aktas, F. Faupel, *Materials* **2019**, 12, 2840.
- [31] S. Veziroglu, M. Z. Ghorri, A. Obermann, K. R  der, O. Polonskyi, T. Strunskus, F. Faupel, O. C. Aktas, *Phys. Status Solidi* **2019**, 216, 1800898.
- [32] A. M. Ferraria, A. P. Carapeto, A. Maria, **2012**, 86, 1988.
- [33] Z. Cheng, S. Zhao, Z. Han, Y. Zhang, X. Zhao, L. Kang, *CrystEng-Comm* **2016**, 18, 8756.
- [34] S. Zhao, Z. Cheng, L. Kang, M. Li, Z. Gao, *RSC Adv.* **2017**, 7, 50064.
- [35] D. N. Pei, L. Gong, A. Y. Zhang, X. Zhang, J. J. Chen, Y. Mu, H. Q. Yu, *Nat. Commun.* **2015**, 6, 2.
- [36] Y. Xu, S. Wu, P. Wan, J. Sun, Z. D. Hood, *RSC Adv.* **2017**, 7, 32461.
- [37] M. Batzill, E. H. Morales, U. Diebold, *Chem. Phys.* **2007**, 339, 36.
- [38] Y. Wang, M. Zhang, S. Lv, X. Li, D. Wang, C. Song, *ACS Omega* **2020**, 5, 13994.
- [39] D. Briggs, in *Handbook of Adhesion*, 2nd ed. (Ed: D. E. Packham), Wiley, New York **2005**, pp. 621–622.
- [40] L. Yang, W. Wang, H. Jiang, Q. Zhang, H. Shan, M. Zhang, K. Zhu, J. Lv, G. He, Z. Sun, *Sens. Actuators B Chem.* **2017**, 242, 932.
- [41] J.-M. Herrmann, *Catal. Today* **1999**, 53, 115.
- [42] T. Zhou, K. Ioannidou, F. J. Ulm, M. Z. Bazant, R. J. M. Pellenq, *Proc. Natl. Acad. Sci. U. S. A.* **2019**, 166, 10652.
- [43] K. Abid, N. H. Belkhir, S. B. Jaber, R. Zribi, M. G. Donato, G. Di Marco, P. G. Gucciardi, G. Neri, R. Ma  lej, *J. Phys. Chem. C* **2020**, 124, 20350.
- [44] J. Shondo, S. Veziroglu, D. Stefan, Y. K. Mishra, T. Strunskus, F. Faupel, O. C. Aktas, *Appl. Surf. Sci.* **2020**, 537, 147795.
- [45] S. Veziroglu, M. Z. Ghorri, M. Kamp, L. Kienle, H. G. Rubahn, T. Strunskus, J. Fiutowski, J. Adam, F. Faupel, O. C. Aktas, *Adv. Mater. Interfaces* **2018**, 5, 1800465.